PCCP

Accepted Manuscript

This is an *Accepted Manuscript*, which has been through the Royal Society of Chemistry peer review process and has been accepted for publication.

Accepted Manuscripts are published online shortly after acceptance, before technical editing, formatting and proof reading. Using this free service, authors can make their results available to the community, in citable form, before we publish the edited article. We will replace this *Accepted Manuscript* with the edited and formatted *Advance Article* as soon as it is available.

You can find more information about *Accepted Manuscripts* in the Information for Authors.

Please note that technical editing may introduce minor changes to the text and/or graphics, which may alter content. The journal's standard Terms & Conditions and the Ethical guidelines still apply. In no event shall the Royal Society of Chemistry be held responsible for any errors or omissions in this *Accepted Manuscript* or any consequences arising from the use of any information it contains.

ROYAL SOCIETY OF CHEMISTRY

www.rsc.org/pccp

Please do not adjust margins

PCCP

ARTICLE

WSe_2 Nanoribbons: New High-performance Thermoelectric Materials

Received 00th January 20xx,
Accepted 00th January 20xx

DOI: 10.1039/x0xx00000x

www.rsc.org/

Kai-Xuan Chen, Zhi-Yong Luo, Dong-Chuan Mo* and Shu-Shen Lyu*

In this work, we first systematically investigate the ballistic transport properties of WSe_2 nanoribbons by using first-principles method. Armchair nanoribbons with narrow ribbon width are mostly semiconductive but the zigzag nanoribbons are metallic. Suprisingly, an enhancement in thermoelectric performance is discovered from monolayer to nanoribbons, especially the armchair ones. The maximum room-temperature thermoelectric figure of merit of 2.2 for armchair nanoribbon can be discovered. This may be contributed to the disorder edge effect, owing to the exsitence of dangling bonds at the ribbon edge. H-passivation is turned out to be a effective way to stablize the edge atoms, which enhances the thermodynamical stablity of the nanoribbons. In addition, after H-passivation, all the armchair nanoribbons exhibit the semiconductive property with similar band gap (~1.3 eV). Our work provides instructional theoretical evidence for the application of armchair WSe_2 nanoribbons as promising thermoelectric materials. The enhancement mechanism of disorder edge effect can also highlight the exploration of achieving outstanding thermoelectric materials.

Introduction

Thermoelectric materials[1], owing to the unique ability to convert heat into electricity and vice versa, have been studied for decades since Seebeck effect (for power generation) and the Peltier effect (for cooling and heat pumping) were discovered in 1800s.[2] Nowadays, the global energy crisis is becoming more and more urgent, the importance of such energy regenerating device is thus emphasized. Thermoelectric figure of merit, as denoted as *ZT*, is a dimensionless parameter used to evaluate the thermoelectric performance of materials, defined as

$$ZT = \frac{GS^2T}{\sigma} \quad (1)$$

where G, S, σ, T are the electronic conductance, Seebeck coefficient, thermal conductance and absolute temperature, respectively. In commercial applications, *ZT* remains around unit for a long time, leading to a low energy conversion efficiency. Even in the frontier researches about high-performance thermoelectric materials, the ZT value is just slightly enhanced. Chung et al. prepared the highly anisotropic material $CsBi_4Te_6$ with ZT of 0.82 at 225K.[3] Tang et al. discovered the high ZT of 1.35 at 300K in Bi_2Te_3 bulk materials with layered nanostructure.[4] In the work of Poudel et al., the ZT value of 1.2 at room temperature can be achieved in a p-type nanocrystalline BiSbTe bulk alloy.[5] To resolve the burning energy issues, new kind of high-performance thermoelectric materials must be discovered and applied.

Recently, rapid development in synthesis and processing of nanoscale materials has provided a new route to design high-performance thermoelectric material since low dimensional materials are predicted to exhibit exceptional properties in comparison with their bulk form.[6] For example, graphene is considered to exhibit extraordinary high thermal conductivity, 5300 $Wm^{-1}K^{-1}$,[7] compared with bulk graphite.

Transition metal Dichalcogenide (TMD)[8, 9], a new emerging family of graphene-like two-dimensional material, has attracted a lot of attention recently due to its application in photoelectric devices[10, 11], field-effect transistors[12, 13], electronics[11, 14], supercapacitors[15], batteries[16], phonon engineering[17], and so on. Typically, TMDs have the molecular form of MX_2 (M=Mo, W; X=S, Se).

Some researches about the thermoelectric properties of this family have been published. Huang et al[18] studied the thermoelectric performance of few layer TMDs and found out that the *ZT* of n-type 1TL-MoS_2 and 2TL-WSe_2 can reach 1.6 and 2.1 at 500 K, respectively (TL is short for trilayer). They also discovered the room-temperature *ZT* of monolayer WSe_2 to be around 0.4.[19] Lee et al[20] used density functional theory to predict that the mixed-layer compounds MS_2/MTe_2 (M = Mo, W) strongly enhance the thermoelectric properties as a consequence of reducing the band gap and the interlayer van der Waals interactions. Fan et al[21] calculated the thermoelectric performance of armchair MoS_2 nanoribbons and approved them as promising thermoelectric materials. It has also been predicted that in this family, WSe_2 is superior than the other members in thermoelectric performance[22]. The question is if WSe_2 nanoribbons (WNRs) would exhibit

School of Chemical Engineering and Technology, Sun Yat-sen University, Guangzhou 510275, China. E-mail: modongch@mail.sysu.edu.cn and lvshsh@mail.sysu.edu.cn; Fax: +86-020-84112150.

Physical Chemistry Chemical Physics Accepted Manuscript

excellent thermoelectric performance, which still remains unclear.

In comparison with intensive researches on the few layer and bulk TMDs[23-26], the study of transport properties on nanoribbons is not satisfactory until now. The object of this article is to explore the thermoelectric transport properties of WSe_2 nanoribbons, to provide theoretical guidance to the design of new high-performance thermoelectric materials.

Model and Method

WSe_2 monolayer[27, 28] has a graphene-like two-dimensional structure including a trilayer "Se-W-Se" sandwich structure. Armchair and zigzag WSe_2 nanoribbons can be imagined as a monolayer to be cut off along specific direction, denoted as AWNR and ZWNR, respectively. Following the conventional notation, AWNR-N_a (ZWNR-N_z) denotes an AWNR (a ZWNR) with N_a(N_z) dimer lines (zigzag chains) across the ribbon width. The schematic illustration of AWNR-N_a and ZWNR-N_z is shown in Fig. 1. At the both end of the nanoribbon (the left and right side in Fig. 1a), dangling bonds exist. After H-passivation, H atoms are added up to stabilize the dangling bonds. An example of AWNR-5 with H-passivation is demonstrated in Fig. 1b and c. And for zigzag WSe_2 nanoribbon, ZWNR-4 with full and partial H-passivation is shown in Fig. 1e and f. In this paper, AWNR-5, -6, -7, -8 without H-passivation (w/o H) and AWNR-4, -5, -6, -7 with H-passivation (with H) as well as ZWNR-4, 5, 6, 7 with partial H-passivation (part H) are under investigation.

For system with length scale along the transport direction smaller than the mean free path (MPF), ballistic assumption is valid.[29] The room-temperature transport properties can be effectively described in ballistic regime. In this article, coherent transport is fully considered while the interactions of electron-electron, electron-phonon and phonon-phonon are not taken into consideration. We use pseudopotential plane wave method to calculate the electronic structure, as implemented in package Quantum Espresso.[30] Density functional theory (DFT) as well as non-equilibrium Green's function (NEGF) method[25] is employed. Norm-conserving pseudopotentials are adopted within the local density approximation (LDA) of Perdew-Zunger with energy (charge density) cutoff up to 50 Ry (500 Ry). The ions minimization is fully done with convergence threshold less than 10^{-4} Ry/bohr on force and 10^{-5} Ry on total energy. The convergence threshold for selfconsistency is set to be 10^{-10} Ry and a vacuum region of 12 Angstroms is used to avoid the periodic image interaction. For vibrational properties, interatomic force constants (IFCs) are performed in the density functional perturbation theory (DFPT) framework. A $1\times1\times7$ Monkhorst-Pack *k*-grid is used to sample the first Brillouin zone for electronic structure. For phonon calculation, the $1\times1\times3$ ($1\times1\times7$) Monkhorst-Pack *q*-grid is adopted for AWNRs (ZWNRs). Maximal localized Wannier functions (MLWFs) method are employed to describe the Bloch functions in Wannier90 package.[31] Once the Hamiltonian matrix and IFCs are obtained, one can work out the physical properties according to the following equations.[32]

For ballistic electron calculation, the retarded Green's function G^r should be obtained firstly.

$$G^r = \left[ES_C - H_C - \Sigma_L^r - \Sigma_R^r \right]^{-1} \quad (2)$$

where E is the electron energy, H_C and S_C are the Hamiltonian and overlap matrix of the central conductor, respectively. Σ_β^r with $\beta = L, R$ denotes the self-energy of the semi-infinite leads, which can be obtained by Eq. (3). Then, the electron transmittance $\mathrm{T}(E)$ can be calculated through Eq. (4).

$$\Sigma_L^r = H_{LC}^\dagger g_L^r H_{LC}\,,\ \Sigma_R^r = K_{CR} g_R^r K_{CR}^\dagger \quad (3)$$

$$\mathrm{T}(E) = \mathrm{Tr}\left(G^r \Gamma_{\mathrm{L}} G^a \Gamma_{\mathrm{R}} \right) \quad (4)$$

where g_L^r and g_R^r are the retarded surface Green's function of

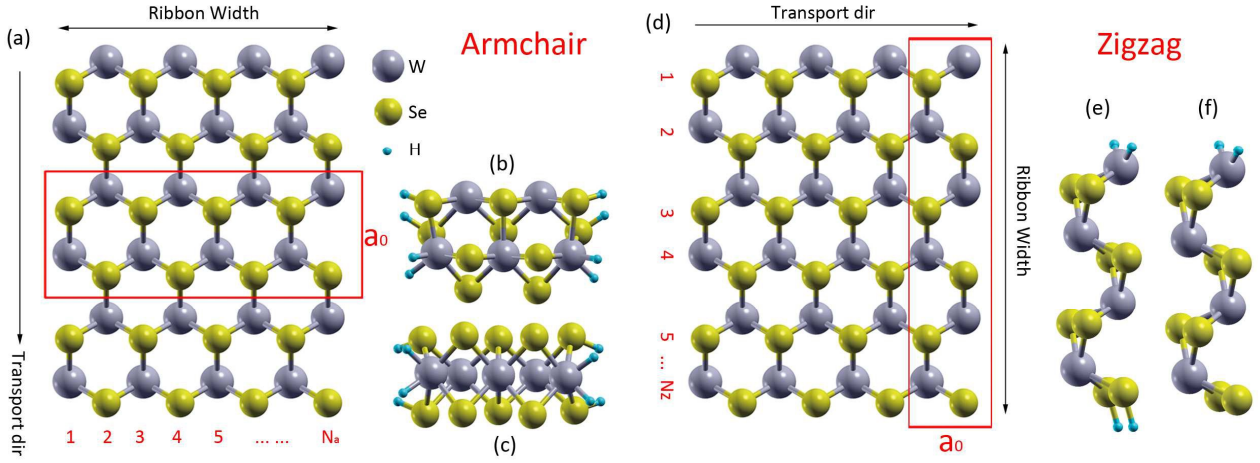

Fig. 1 (a) the schematic illustration of armchair WSe_2 nanoribbon in top view. The unitcell of AWNR-N_a is denoted by the red solid box in which N_a defines the ribbon width. The unitcell of AWNR-5 with H-passivation is shown as an example in (b) oblique view and (c) front view. (d) shows the structure of zigzag WSe_2 nanoribbon with the unitcell denoted by the red solid box. The definition of N_z is a little different from that of N_a. The ZWNR-4 with full and partial H-passivation in shown in (e) and (f), respectively.

Physical Chemistry Chemical Physics Accepted Manuscript

This journal is © The Royal Society of Chemistry 20xx

Please do not adjust margins

the left and right lead, respectively. $G^a = \left(G^r\right)^\dagger$ is the advanced Green's function and $\Gamma_\beta = i\left(\Sigma_\beta^r - \Sigma_\beta^a\right)$ with $\beta = L, R$ describes the interaction between the leads and the central conductor.

Next, for convenience, Lorenz function is introduced to calculate the electronic conductance *G*, Seebeck coefficient *S*, electronic thermal conductance σ_{el} according to Eqs. (5)-(8).

$$L_n(\mu,T) = \frac{2}{h}\int dE \mathrm{T}(E) \times (E-\mu)^n \times \left[-\frac{\partial f(E,\mu,T)}{\partial E}\right] \quad (5)$$

$$G = q^2 L_0 \quad (6)$$

$$S = \frac{1}{qT} \times \frac{L_1}{L_0} \quad (7)$$

$$\sigma_{el} = \frac{1}{T} \times \left(L_2 - \frac{L_1^2}{L_0}\right) \quad (8)$$

where $f(E, \mu, T)$ is the Fermi-Dirac distribution function, μ is the chemical potential and T is the absolute temperature. Besides, h is the Planck constant and q is the charge of electron.

For ballistic phonon calculation, one just needs to replace the ES_C with $(\omega + i\eta)^2$ and the H_C with K_C in Eq. (2) to obtain the phonon transmittance $\mathrm{T}(\omega)$, where ω is the phonon frequency and η is an infinitesimal added as the imaginary part of ω. After then, the phononic thermal conductance σ_{ph} can be calculated through Eq. (9).

$$\sigma_{ph}(T) = \frac{\hbar}{2\pi}\int_0^\infty \mathrm{T}(\omega)\omega\frac{\partial f(\omega,T)}{\partial T}d\omega \quad (9)$$

where $f(\omega, T)$ is the Bose-Einstein distribution function, and $\hbar$ is the reduced Planck constant.

Finally, the value of ZT can be figured out from Eq. (1) after all thermoelectric factors above are obtained where thermal conductance can be contributed both from electrons and phonons.

$$\sigma = \sigma_{el} + \sigma_{ph} \quad (10)$$

Results and Discussion

Electronic structures

To start with, we study the electronic structure of WNRs, since the electronic structure of the system usually dominates the physical properties. Density functional theory usually underestimates the bandgap value of electronic structure. However, in the previous studies, it was pointed out that in the case of transition metal dichalcogenides, LDA can provide the accurate bandgap values, which is also confirmed in our previous work. The WSe_2 monolayer has been predicted to be semiconductor with wide band gap of ~1.7 eV in the previous researches,[11, 23, 25] consistent with the experimental data.[18, 33] That is exactly the reason why LDA pseudopotentials are adopted in our simulation work. Monolayer WSe_2 is discovered to have extraordinary electronic properties. Kaloni et al. discovered the quantum spin Hall effect in graphene sandwiched between WS_2 and WSe_2 monolayers in the absence of magnetic field.[34] Amin et al. used first-principles method to investigate the electronic properties of MoS_2-WSe_2 heterostructure and found out the semiconductive property.[35] Interestingly, its corresponding armchair nanoribbons show quite different feature, especially the narrow-width ones. Peculiarly AWNR-5 is figured out to be metallic. As ribbon width increases, a metal-semiconductor transition appears, as shown in Fig. 2. However, small band gaps have been confirmed in these AWNRs, compared with the WSe_2 monolayer. This may be contributed from the disorder edge effect. For AWNRs, dangling bonds exist at the ribbon edge. The existence of lonely electrons at unsaturated dangling bonds will lead to the generation of extra energy level around the Fermi surface in band structure, just like n-doped effect. The disorder edge effect becomes more intensive in narrower ribbon since the proportion of lonely electrons increases. After the introduction of H-passivation, lonely electrons disappear and so as the extra energy levels. As expected, the band gap becomes wider. Surprisingly, the value of band gap of all the AWNRs with H-passivation stays almost the same, fluctuating around 1.3 eV. To be specific, the values are listed out in Table 1.

Table 1 The lattice parameters[a] (Å) and electronic band gap (eV) of the calculated WSe_2 nanoribbons

	Nanoribbons	Lattice parameter a_0	Bandgap
w/o H-passivation	AWNR-5	5.590	metallic
	AWNR-6	5.556	0.35
	AWNR-7	5.586	0.52
	AWNR-8	5.591	0.5
with H-passivation	AWNR-4	5.502	1.23
	AWNR-5	5.584	1.28
	AWNR-6	5.603	1.31
	AWNR-7	5.598	1.29
w/o H-passivation	ZWNR-4	3.200	metallic
	ZWNR-5	3.210	metallic
	ZWNR-6	3.218	metallic
with partial H-passivation	ZWNR-4	3.226	metallic
	ZWNR-5	3.240	metallic
	ZWNR-6	3.234	metallic
	ZWNR-7	3.242	metallic

[a]The lattice parameter a_0 is defined in Fig. 1.

Table 2 The bond covalency (eV) of W-Se pair for the calculated WSe2 nanoribbons

	Nanoribbons	Covalency (eV)
w/o H-passivation	AWNR-5	-2.11
	AWNR-6	-1.46
	AWNR-7	-1.15
	AWNR-8	-1.54
with H-passivation	AWNR-4	-2.68
	AWNR-5	-2.20
	AWNR-6	-2.02
	AWNR-7	-1.74

Physical Chemistry Chemical Physics Accepted Manuscript

The electronic structure of zigzag WSe_2 nanoribbons is shown in Fig. 3. It can be clearly seen that the electronic subbands pass through the Fermi surface in zigzag nanoribbons without H-passivation, resulting in the metallic property. After partial H-passivation, less subbands exist around the Fermi energy but still remain the metallic property, which is similar to the research of Botello-Mendez[36] on MoS_2 nanoribbons.

We then study the bond covalency of W-Se pair of the armchair nanoribbons, according to the method described in the previous references.[37-39] as shown in Table 2. In the supporting information we show that the highest occupied valence subbands and the lowest unoccupied conduction subbands are mainly attributed to the *p* orbitals from Se atoms and the *d* orbitals from W atoms. Thus, we just need to consider the bond covalency between *d* levels from W atoms and *p* levels from Se atoms by considering the energy range of [-10.0, 10.0] eV. As nanoribbon width increases, the bond covalency of W-Se pair of the armchair nanoribbons increase as well, except for AWNR-8 without H-passivation. This would indicate the existence of higher covalency with increasing ribbon width. In addition, the H-passivation seems to reduce the covalency of the W-Se pair slightly.

Phonon dispersion and transport properties

The phonon dispersion of AWNR-5, 6, 7 is plotted in Fig. 4a.

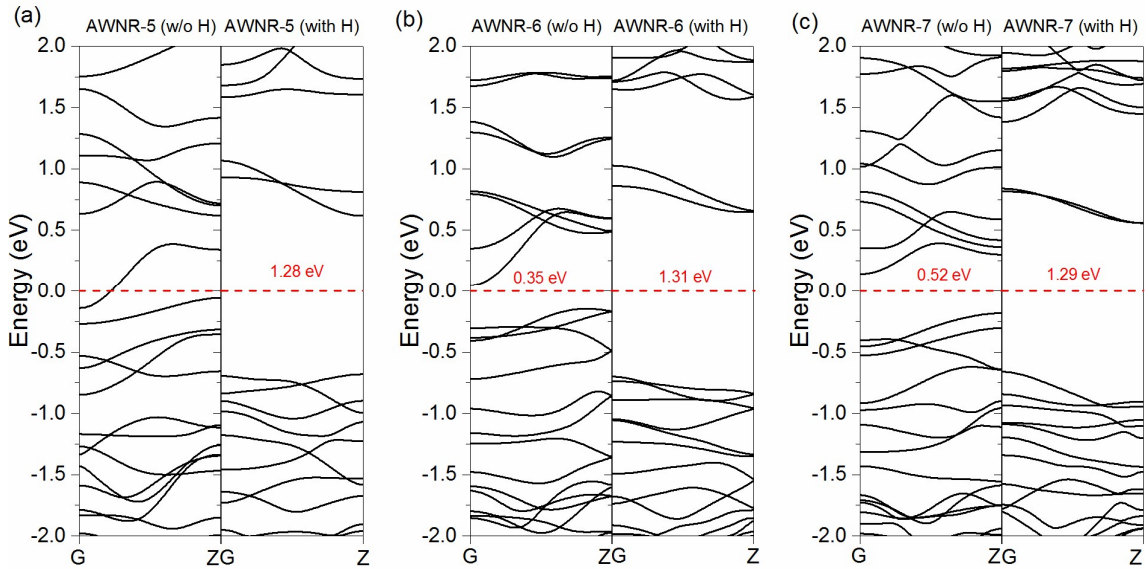

Fig. 2 The electronic band structure along the high symmetry point "G (0, 0, 0) - Z (0, 0, 0.5)" of (a) AWNR-5, (b) AWNR-6, (c) AWNR-7 without and with H-passivation. The red numbers inside the figure denote the band gap value of the corresponding structures.

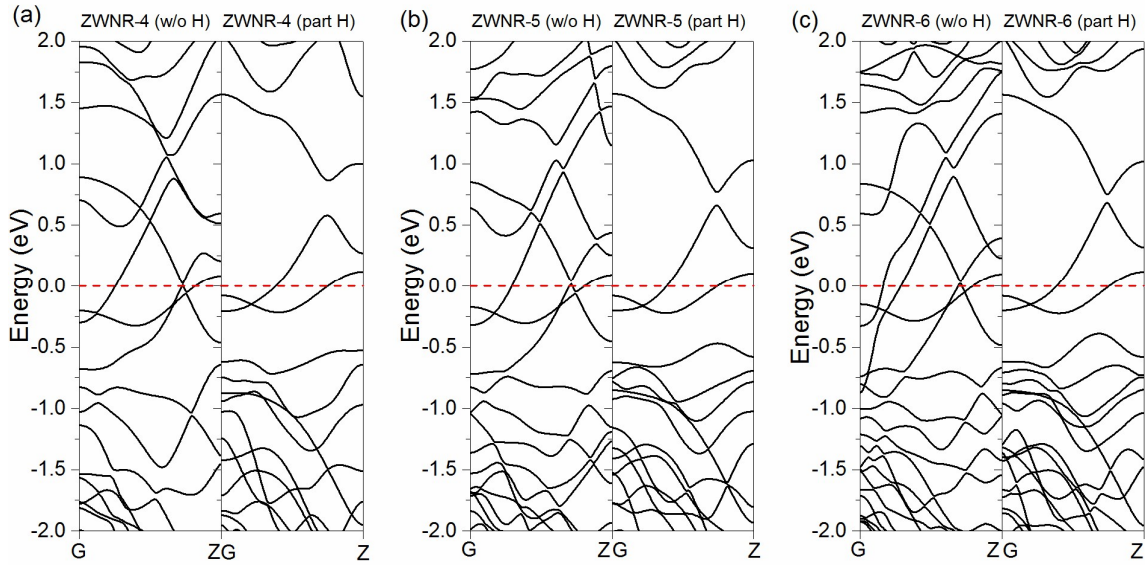

Fig. 3 The electronic band structure along the high symmetry point "G (0, 0, 0) - Z (0, 0, 0.5)" of (a) ZWNR-4, (b) ZWNR-5, (c) ZWNR-6 without and with partial H-passivation.

Physical Chemistry Chemical Physics Accepted Manuscript

This journal is © The Royal Society of Chemistry 20xx

Please do not adjust margins

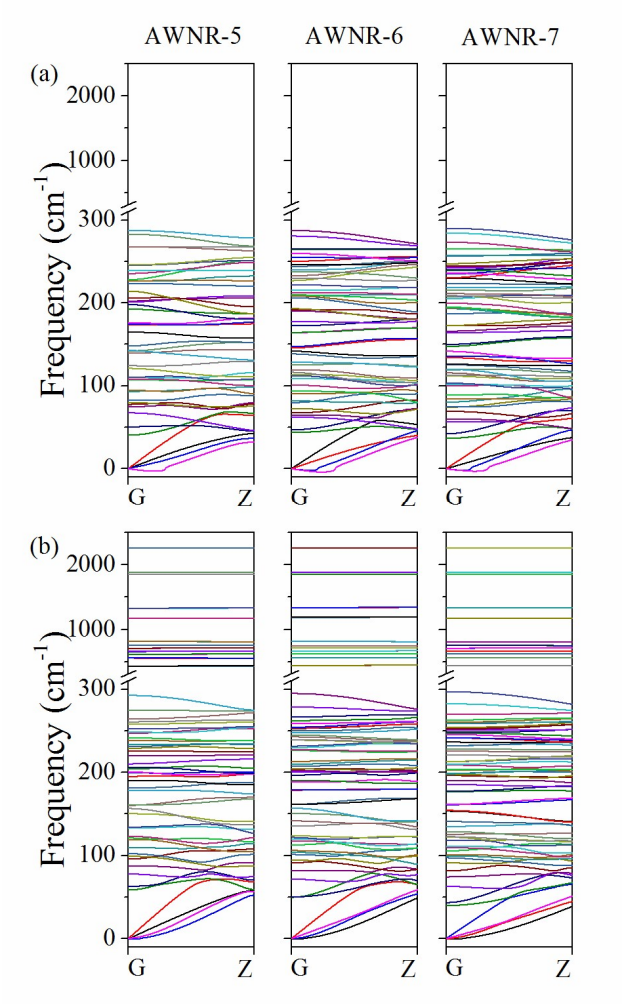

Fig. 4 The phonon dispersion plots along the high symmetry point "G (0, 0, 0) - Z (0, 0, 0.5)" of AWNR-5, -6, -7 (a) without H-passivation and (b) with H-passivation.

For one-dimensional material such as nanoribbon, there are supposed to be four acoustic phonon branches at the Gamma point of Brillouin zone. It can be also observed that there exist some imaginary frequency modes (frequency < 0 cm^{-1}). The existence of imaginary frequency usually indicates the meta-stable state of the system if the requirement of calculation accuracy is met. In our case, it may be related to the disorder caused by the dangling bonds at the ribbon edge. Such phenomenon has been found and illustrated in the previous researches of graphene nanoribbon with disorder at ribbon edge.[29] The cutoff frequency of these nanoribbons is around 300 cm^{-1}, consistent with previous study on the strain engineering of the monolayer WSe_2.[40] For the sake of comparison, the phonon dispersion of AWNR-5, 6, 7 after H-passivation is demonstrated as well in Fig. 4b. The introduction of H-passivation stabilizes the dangling bonds at ribbon edge and thus reduces the disorder edge effect. After H-passivation, the low-frequency acoustic modes should be altered that no imaginary frequency appear. The foreign H atoms not only eliminate the imaginary frequency, but also increase the cutoff

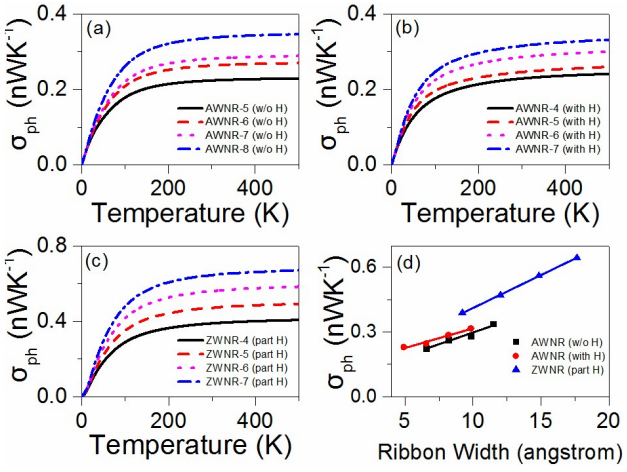

Fig. 5 The phononic thermal conductance of AWNRs (a) without and (b) with H-passivation, (c) ZWNRs with partial H-passivation as a function of absolute temperature. (d) The room-temperature phononic thermal conductance versus nanoribbon width. Data shown are for AWNR-5, 6, 7, 8 without H-passivation, AWNR-4, 5, 6, 7 with H-passivation and ZWNR-4, 5, 6, 7 with partial H-passivation: linear fits have correlation coefficients 0.946, 0.969 and 1.000, respectively. Slopes of the linear fits are 0.219, 0.183 and 0.305 $Wm^{-1}K^{-1}$, while vertical intercepts are 0.0790, 0.134 and 0.106 nWK^{-1}, respectively.

phonon frequency from 300 cm^{-1} (pristine) to 2300 cm^{-1}(with H-passivation). The high frequency modes (> 300 cm^{-1}) result from the vibration mode of H atoms while the low frequency modes (< 300 cm^{-1}) are only slightly altered. The room-temperature properties are mainly dominated by the low-frequency phononic modes since the high-frequency modes cannot be activated in low temperature.

The phonon dispersion of ZWNR-4 is demonstrated in the supporting information. We consider three cases: without H-passivation, with partial H-passivation and with full H-passivation. Only those with partial H-passivation show the negligible imaginary frequency and that is why only this type of ZWNRs are investigated in our paper.

The phononic thermal conductance is plotted as a function of absolute temperature in Fig. 5a-c. As expected, the value increases with increasing temperature since more available phonon modes are activated at higher temperature. As ribbon width increases, the number of total atoms in the unitcell increases as well, which leads to more phonon channels at certain frequency. For ballistic transport, the phononic thermal conductance is determined by the number of available phonon channels.[41] Therefore, the regularity is to be seen that the phononic thermal conductance is positively proportional to the ribbon width, for nanoribbons either without or with H-passivation.

The phononic thermal conductance of zigzag nanoribbons is much bigger than that of armchair counterparts, which is consistent with the research of Jiang[42] on MoS_2 nanoribbons. The room-temperature phononic thermal conductance of AWNRs with and without H-passivation as well as ZWNRs with partial H-passivation versus ribbon width is demonstrated in Fig. 5d, in which the linear fitness coefficient is 0.946, 0.969 and 1.000, respectively. The slope of the linear fits defines the

Physical Chemistry Chemical Physics Accepted Manuscript

thermal conductance increase per unit ribbon width. The value is about 0.18~0.22 (0.31) $Wm^{-1}K^{-1}$ for AWNRs (ZWNRs), significantly smaller than that of 0.7~1.2 $Wm^{-1}K^{-1}$ for graphene naoribbons.[29] The positive contribution to the thermal conductance originates from disorder edge effect is about 0.1 nWK^{-1} on extrapolating the linear trends to ribbon width equal to zero.

Thermoelectric properties

In this part, we will focus on the thermoelectric transport properties of the WNRs. As pointed out in the electronic part, AWNR-5 is supposed to be metallic, i.e., the electrons from the valence subbands can be excited into the conductance subbands when the chemical potential is located at the Fermi energy. It can be seen directly from Fig. 6a and d that the electronic thermal conductance of AWNR-5 have positive value. The maximum Seebeck coefficient usually depends on electronic band gap.[21] After the introduction of H-passivation, the behaviour of thermoelectric factors of AWNRs with different ribbon width trends to converge, resulting from the similar electronic band gap as stated in the previous part.

In the work of Fan et al.,[21] armchair MoS_2 nanoribbons are discovered to exhibit excellent thermoelectric performance. Now we turn to the study of WSe_2 nanoribbons since in our previous study, we observe that monolayer WSe_2 is superior than monolayer MoS_2 in thermoelectric performance. Fig. 6c and f show the thermoelectric figure of merit versus chemical potential at room temperature. The disorder edge effect leads to the structure reconstruction at the ribbon edge. This may be the origin of the enhancement in thermoelectric performance. The maximum room-temperature *ZT* can reach by 2.2 for AWNR-6. This value is almost enhanced by three times compared with the WSe_2 monolayer (~0.8 at 300 K[25]), which can be competitive with the most excellent thermoelectric materials in the world. After the introduction of H-passivation, a wide gap emerges, corresponding to the wide electronic band gap. Besides, the maximum *ZT* is reduced since the disorder edge effect is weakened since the H-passivation stabilizes the dangling bonds. It confirms our suspect that the origin of the enhancement mechanism of thermoelectric performance comes from the disorder edge effect induced by dangling bonds at the ribbon edge.

The thermoelectric factors of ZWNRs with partial H-passivation are shown in Fig. 7. The Seebeck coefficient is obviously smaller than that of AWNRs, resulting from the zero band gap nature from the electronic structure. A reduce in Seebeck coefficient would certainly lead to a decrease in thermoelectric performance. The *ZT* of these ZWNRs is much smaller than that of AWNRs. As ribbon width increases, the *ZT* decreases and the maximum value for ZWNR-4 with partial H-passivation is only 0.92.

Finally, we study the temperature dependence of *ZT* in AWNRs in the range of 50~500 K, as plotted in Fig. 8. As temperature increases, *ZT* is usually supposed to increase as well since the definition of *ZT* has a *T* in it. For AWNRs without

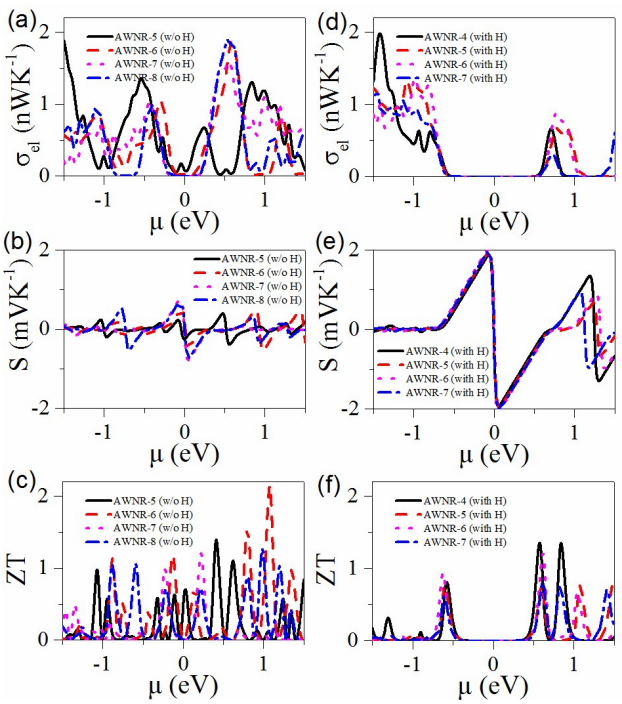

Fig. 6 The room-temperature electronic thermal conductance, Seebeck coefficient and thermoelectric figure of merit of (a, b, c) AWNR-5, -6, -7, -8 without H-passivation and (d, e, f) AWNR-4, -5, -6, -7 with H-passivation plotted as a function of chemical potential, respectively.

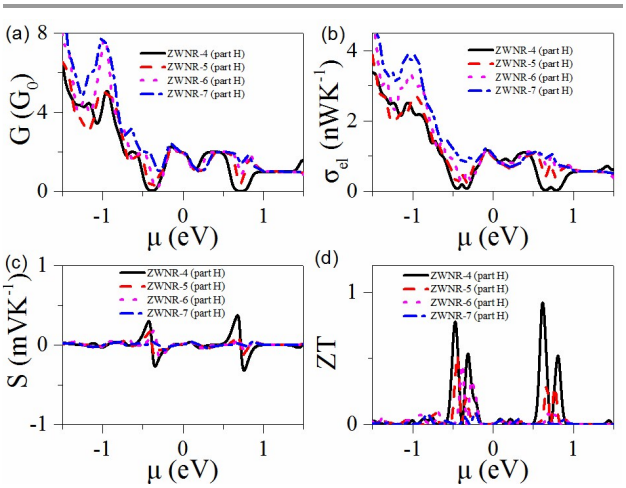

Fig. 7 The room-temperature thermoelectric factors as a function of chemical potential: (a) electronic conductance; (b) electronic thermal conductance; (c) Seebeck coefficient; (d) thermoelectric figure of merit.

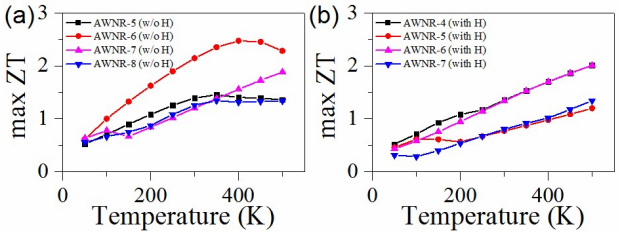

Fig. 8 The temperature dependence of maximum thermoelectric figure of merit of AWNRs (a) without H-passivation and (b) with H-passivation.

Physical Chemistry Chemical Physics Accepted Manuscript

This journal is © The Royal Society of Chemistry 20xx

Please do not adjust margins

H-passivation, however, a peak value can be achieved (the peak value for AWNR-7 is not shown here since it locates at temperature higher than 500 K). AWNR-6 without H-passivation seems to exhibit the most excellent thermoelectric performance. The most effective operating temperature lies at 400 K, with a *ZT* of 2.5.

Conclusions

In summary, density functional theory as well as ballistic non-equilibrium Green's Function method is employed to investigate the transport properties of armchair and zigzag WSe_2 nanoribbons (AWNRs and ZWNRs). AWNR-5, -6, -7, -8 without H-passivation and AWNR-4, -5, -6, -7 with H-passivation as well as ZWNR-4, 5, 6, 7 with partial H-passivation are under investigation. The phononic thermal conductance of these nanoribbons shows a good linear fitness with regard to ribbon width (correlation coefficients are 0.946, 0.969 and 1.000, respectively). Due to the disorder edge effect, AWNRs are figured out to possess higher room-temperature *ZT* than ZWNRs. The maximum *ZT* of 2.2 for AWNR-6 without H-passivation can be discovered. The introduction of H-passivation stabilizes the dangling bond at the ribbon edge, leading to a decrease in *ZT*, which confirms our suspect that the enhancement mechanism of thermoelectric performance origins from the disorder edge effect. The optimal operating temperature for the nanoribbons without H-passivation is furthermore figured out to be around 400 K. With advances in experimental techniques, it is possible that these pristine and hydrogen-passivated nanoribbons will be fabricated, maybe like the graphene nanoribbons[43] or the MoS_2 nanoribbons[44, 45]. Therefore our first-principles calculation work aims to provide valuable theoretical guidance for exploring high-performance nanostructured thermoelectric materials in experiments of transition metal dichalcogenides.

Acknowledgements

Financial support from the National Natural Science Foundation of China (Grant No. 51276202), Special Program for Applied Research on Super Computation of the NSFC-Guangdong Joint Fund (the second phase) and the Fundamental Research Funds for the Central Universities are gratefully acknowledged. The simulation work is supported by the National Supercomputer Center in Guangzhou and the high-performance grid computing platform of Sun Yat-sen University.

Notes and references

1. M. He, F. Qiu and Z. Q. Lin, *Energ. Environ. Sci.*, 2013, **6**, 1352-1361.
2. G. Chen, M. S. Dresselhaus, G. Dresselhaus, J. P. Fleurial and T. Caillat, *Int. Mater. Rev.*, 2003, **48**, 45-66.
3. D. Y. Chung, T. P. Hogan, M. Rocci-Lane, P. Brazis, J. R. Ireland, C. R. Kannewurf, M. Bastea, C. Uher and M. G. Kanatzidis, *J. Am. Chem. Soc.*, 2004, **126**, 6414-6428.
4. X. Tang, W. Xie, H. Li, W. Zhao, Q. Zhang and M. Niino, *Appl. Phys. Lett.*, 2007, **90**, 012102.
5. B. Poudel, Q. Hao, Y. Ma, Y. Lan, A. Minnich, B. Yu, X. Yan, D. Wang, A. Muto, D. Vashaee, X. Chen, J. Liu, M. S. Dresselhaus, G. Chen and Z. Ren, *Science*, 2008, **320**, 634-638.
6. J. F. Li, W. S. Liu, L. D. Zhao and M. Zhou, *Npg Asia Mater*, 2010, **2**, 152-158.
7. A. A. Balandin, S. Ghosh, W. Bao, I. Calizo, D. Teweldebrhan, F. Miao and C. N. Lau, *Nano Lett.*, 2008, **8**, 902-907.
8. X. Huang, Z. Zeng and H. Zhang, *Chem. Soc. Rev.*, 2013, **42**, 1934-1946.
9. M. Chhowalla, H. S. Shin, G. Eda, L. J. Li, K. P. Loh and H. Zhang, *Nat. Chem.*, 2013, **5**, 263-275.
10. J. Lu, A. Carvalho, X. K. Chan, H. Liu, B. Liu, E. S. Tok, K. P. Loh, A. H. Castro Neto and C. H. Sow, *Nano Lett.*, 2015, **15**, 3524-3532.
11. Q. H. Wang, K. Kalantar-Zadeh, A. Kis, J. N. Coleman and M. S. Strano, *Nat Nanotechnol*, 2012, **7**, 699-712.
12. V. Podzorov, M. E. Gershenson, C. Kloc, R. Zeis and E. Bucher, *Appl. Phys. Lett.*, 2004, **84**, 3301-3303.
13. A. Nourbakhsh, A. Zubair, M. S. Dresselhaus and T. Palacios, *Nano Lett.*, 2016, **16**, 1359-1366.
14. J. Huang, W. Wang, Q. Fu, L. Yang, K. Zhang, J. Zhang and B. Xiang, *Nanotechnology*, 2016, **27**, 13LT01.
15. H. Tang, J. Wang, H. Yin, H. Zhao, D. Wang and Z. Tang, *Adv. Mater.*, 2015, **27**, 1117-1123.
16. H. Liu, D. W. Su, R. F. Zhou, B. Sun, G. X. Wang and S. Z. Qiao, *Adv. Energy. Mater.*, 2012, **2**, 970-975.
17. J. W. Jiang, *Nanoscale*, 2014, **6**, 8326-8333.
18. W. Huang, X. Luo, C. K. Gan, S. Y. Quek and G. Liang, *Phys. Chem. Chem. Phys.*, 2014, **16**, 10866-10874.
19. W. Huang, H. Da and G. Liang, *J. Appl. Phys.*, 2013, **113**, 104304.
20. C. Lee, J. Hong, M.-H. Whangbo and J. H. Shim, *Chem. Mater.*, 2013, **25**, 3745-3752.
21. D. D. Fan, H. J. Liu, L. Cheng, P. H. Jiang, J. Shi and X. F. Tang, *Appl. Phys. Lett.*, 2014, **105**, 133113.
22. S. Kumar and U. Schwingenschlögl, *Chem. Mater.*, 2015, **27**, 1278-1284.
23. H. Sahin, S. Tongay, S. Horzum, W. Fan, J. Zhou, J. Li, J. Wu and F. M. Peeters, *Phys. Rev. B*, 2013, **87**, 165409.
24. D. Wickramaratne, F. Zahid and R. K. Lake, *J. Chem. Phys.*, 2014, **140**, 124710.
25. K. X. Chen, X. M. Wang, D. C. Mo and S. S. Lyu, *J Phys Chem C*, 2015, **119**, 26706-26711.
26. X. Su, W. Ju, R. Zhang, C. Guo, J. Zheng, Y. Yong and X. Li, *RSC Adv.*, 2016, **6**, 18319-18325.
27. K. Xu, Z. Wang, X. Du, M. Safdar, C. Jiang and J. He, *Nanotechnology*, 2013, **24**, 465705.
28. J. K. Huang, J. Pu, C. L. Hsu, M. H. Chiu, Z. Y. Juang, Y. H. Chang, W. H. Chang, Y. Iwasa, T. Takenobu and L. J. Li, *ACS Nano*, 2014, **8**, 923-930.
29. Z. W. Tan, J. S. Wang and C. K. Gan, *Nano Lett.*, 2011, **11**, 214-219.
30. P. Giannozzi, S. Baroni, N. Bonini, M. Calandra, R. Car, C. Cavazzoni, D. Ceresoli, G. L. Chiarotti, M. Cococcioni, I. Dabo, A. Dal Corso, S. de Gironcoli, S. Fabris, G. Fratesi, R. Gebauer, U. Gerstmann, C. Gougoussis, A. Kokalj, M. Lazzeri, L. Martin-Samos, N. Marzari, F. Mauri, R. Mazzarello, S. Paolini, A. Pasquarello, L. Paulatto, C. Sbraccia, S. Scandolo, G. Sclauzero, A. P. Seitsonen, A. Smogunov, P. Umari and R. M. Wentzcovitch, *J. Phys.: Condens. Matter*, 2009, **21**, 395502.
31. A. A. Mostofi, J. R. Yates, Y. S. Lee, I. Souza, D. Vanderbilt and N. Marzari, *Comput. Phys. Commun.*, 2008, **178**, 685-699.

Physical Chemistry Chemical Physics Accepted Manuscript

32. R. D'Agosta, *Phys. Chem. Chem. Phys.*, 2013, **15**, 1758-1765.
33. C. H. Chang, X. F. Fan, S. H. Lin and J. L. Kuo, *Physical Review B*, 2013, **88**, 195420.
34. T. P. Kaloni, L. Kou, T. Frauenheim and U. Schwingenschlögl, *Appl. Phys. Lett.*, 2014, **105**, 233112.
35. B. Amin, T. P. Kaloni, G. Schreckenbach and M. S. Freund, *Appl. Phys. Lett.*, 2016, **108**, 063105.
36. A. R. Botello-Mendez, F. Lopez-Urias, M. Terrones and H. Terrones, *Nanotechnology*, 2009, **20**, 325703.
37. A. Cammarata and T. Polcar, *Inorg. Chem.*, 2015, **54**, 5739-5744.
38. A. Cammarata and J. M. Rondinelli, *J. Chem. Phys.*, 2014, **141**, 114704.
39. A. Cammarata and T. Polcar, *RSC Adv.*, 2015, **5**, 106809-106818.
40. B. Amin, T. P. Kaloni and U. Schwingenschlögl, *RSC Advances*, 2014, **4**, 34561.
41. J. W. Jiang, J. S. Wang and B. W. Li, *J. Appl. Phys.*, 2011, **109**, 014326.
42. J. W. Jiang, X. Zhuang and T. Rabczuk, *Sci Rep*, 2013, **3**, 2209.
43. X. Li, X. Wang, L. Zhang, S. Lee and H. Dai, *Science*, 2008, **319**, 1229-1232.
44. X. Liu, T. Xu, X. Wu, Z. Zhang, J. Yu, H. Qiu, J. H. Hong, C. H. Jin, J. X. Li, X. R. Wang, L. T. Sun and W. Guo, *Nat Commun*, 2013, **4**, 1776.
45. Z. Wang, H. Li, Z. Liu, Z. Shi, J. Lu, K. Suenaga, S. K. Joung, T. Okazaki, Z. Gu, J. Zhou, Z. Gao, G. Li, S. Sanvito, E. Wang and S. Iijima, *J. Am. Chem. Soc.*, 2010, **132**, 13840-13847.

Physical Chemistry Chemical Physics Accepted Manuscript

This journal is © The Royal Society of Chemistry 20xx